ACS APPLIED MATERIALS & INTERFACES

Research Article

www.acsami.org

Polarization Energies at Organic–Organic Interfaces: Impact on the Charge Separation Barrier at Donor–Acceptor Interfaces in Organic Solar Cells

Sean M. Ryno,[†,∥] Yao-Tsung Fu,[∥] Chad Risko,[*,#] and Jean-Luc Brédas[*,†]

[†]Solar and Photovoltaics Engineering Research Center, King Abdullah University of Science and Technology, Thuwal 23599-6900, Kingdom of Saudi Arabia

[∥]School of Chemistry and Biochemistry & Center for Organic Photonics and Electronics, Georgia Institute of Technology, Atlanta, Georgia 30332-0400, United States

[#]Department of Chemistry & Center for Applied Energy Research, University of Kentucky, Lexington, Kentucky 40506-0055, United States

Supporting Information

ABSTRACT: We probe the energetic landscape at a model pentacene/fullerene (C_{60}) interface to investigate the interactions between positive and negative charges, which are critical to the processes of charge separation and recombination in organic solar cells. Using a polarizable force field, we find that polarization energy, i.e., the stabilization a charge feels due to its environment, is larger at the interface than in the bulk for both a positive and a negative charge. The combination of the charge being more stabilized at the interface and the Coulomb attraction between the charges results in a barrier to charge separation at the pentacene/C_{60} interface that can be in excess of 0.7 eV for *static* configurations of the donor and acceptor locations. However, the impact of molecular motions, i.e., the dynamics, at the interface at room temperature results in a distribution of polarization energies and in charge separation barriers that can be significantly reduced. The dynamic nature of the interface is thus critical, with the polarization energy distributions indicating that sites along the interface shift in time between favorable and unfavorable configurations for charge separation.

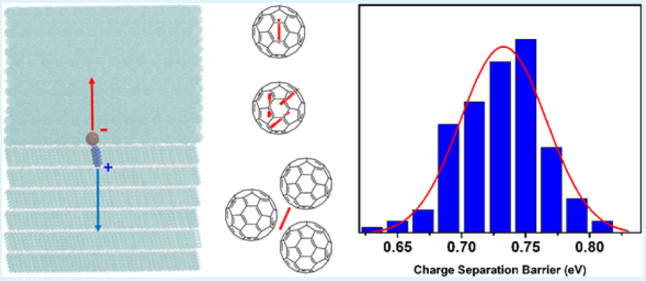

KEYWORDS: *organic photovoltaics, charge separation and recombination, polarization, organic–organic interfaces, molecular dynamics, multiscale modeling, energetic disorder*

INTRODUCTION

Organic photovoltaics (OPV) hold promise of providing large-area, low-cost solar energy conversion, with current multijunction devices exceeding 13% power conversion efficiency[1,2] and single-layer devices now approaching 12%.[3−5] The active layers of these devices typically consist of two components, an electron donor and an electron acceptor, either in a bilayer structure or as a blend termed a bulk heterojunction. Morphology plays a critical role in the efficiencies of the various electronic and optical processes involved in solar-cell operation, including optical absorption, exciton formation, exciton migration, exciton dissociation, charge recombination, charge transport, and charge collection.[6] While the importance of the donor–acceptor interface has been acknowledged in previous investigations,[7−15] of particular focus over the past few years has been the purity of the interface between the two materials. What was once thought to be fairly clear-cut interfaces between the donor and acceptor components has been replaced by a complex morphological picture that includes pure domains with different extents of ordered and disordered packing as well as intermixed regions of the two materials where charge generation primarily occurs.[16−28]

As we discussed recently,[29] the energetic landscape at a surface (i.e., organic–vacuum interface) differs significantly from the bulk of a crystalline material. Furthermore, one would expect the addition of a second organic component to further complicate the landscape. In the bulk of an organic molecular crystal or at an organic–vacuum interface, all molecular sites are essentially identical, except for the difference in site energies due to nonequivalent molecules and dynamic fluctuations. In contrast, at organic–organic interfaces, the molecular sites reside in distinct environments, which will result in a distribution of site energies or polarization energies. Because of the anisotropic nature of the environment, the barrier to charge separation is expected to vary from molecular site to molecular site. Here, in order to better understand the

Received: March 7, 2016
Accepted: May 31, 2016
Published: May 31, 2016

DOI: 10.1021/acsami.6b02851
ACS Appl. Mater. Interfaces 2016, 8, 15524–15534

environment of charge carriers at the donor−acceptor interface and to determine the impact of molecular motions on the charge separation process, we use a combination of molecular dynamics (MD) simulations together with the methodology we developed[21,30,31] for determining electronic polarization energy in organic molecular crystals. Our goal is to gain a picture of the energetic landscape at a disordered donor−acceptor interface and to investigate the landscape dynamics, i.e., how it changes with time.

We take the pentacene/C_{60} interface as a representative model; see Figure 1. It is useful to recall that Verlaak et al. showed previously, using a static (i.e., fixed) configuration of the interface, that an ideal *edge-on* pentacene (001)/C_{60} interface presents a barrier of approximately 0.4 eV to charge separation, while charge separation at a *face-on* pentacene(01−1)/C_{60} interface is quasi-barrierless, leading one to assume that the *face-on* orientation is preferable.[12] Yi et al.,[11] however, underlined that this is not necessarily the case, as the rate of charge recombination is calculated to be several orders-of-magnitude faster for the *face-on* orientation than the *edge-on* orientation.

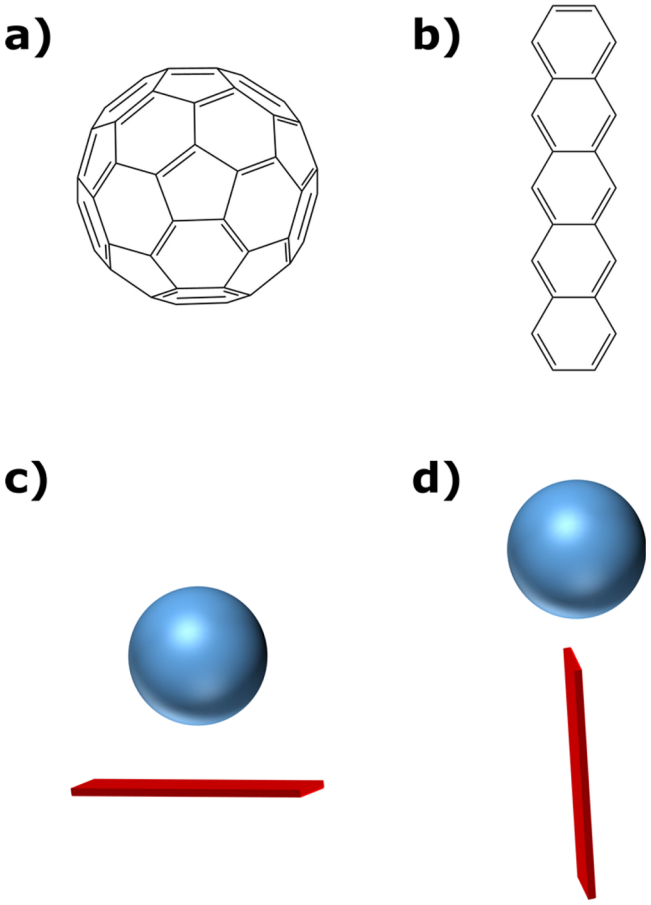

Figure 1. Chemical structures of the C_{60} fullerene (a) and pentacene (b). Graphical representations of the (c) *face-on* pentacene/C_{60} and (d) *edge-on* pentacene/C_{60} complexes.

This work is structured as follows. We begin by determining the polarization energy of a positive charge carrier in bulk pentacene and a negative charge carrier in bulk C_{60} and obtain good agreement with experiment. To assess the impact of molecular orientation at an interface, we then consider model interfaces where pentacene is either *face-on* or *edge-on*. Finally, we examine a bilayer interface composed of bulk pentacene and C_{60} to assess the polarization energy at molecular sites along the interface and into the bulk; we do so for not only static but also dynamic frameworks to determine how the polarization energy varies as a function of time. At sites along the interface, we evaluate the geminate pair energies, i.e., when the charges are allowed to interact, and the noninteracting electron−hole energies, i.e., the change in the energy of the system due to the presence of the hole and electron when they are unable to see each other, to examine the fluctuations with time of the barrier to charge separation.

METHODOLOGY

All polarization energies were calculated via the AMOEBA force field of Ren and Ponder.[32,33] The geometries of isolated pentacene molecules used for the AMOEBA force field parametrization, one-dimensional, stacked interfaces, and the unit cells that were replicated and from which spherical bulk clusters and slabs were extracted, for bulk and interfacial systems, respectively, were obtained from the Cambridge Structural Database (PENCEN04).[34,35] The Materials Studio 6.1 software suite was used to create a face-centered cubic C_{60} packing configuration where $\alpha = \beta = \gamma = 60°$ and $a = b = c = 9.943$ Å for the reduced cell and $\alpha = \beta = \gamma = 90°$ and $a = b = c = 14.062$ Å for the conventional cell, mirroring the unit cell parameters reported by Ibers and co-workers (SOCTOT23) without the positional disorder present in the reported crystal structure.[36]

To generate force field parameters, atom-centered multipoles were obtained with Stone's GDMA program via distributed multipole analysis of the single-particle density matrices.[37] To derive the density matrices, single-point energy calculations at the MP2/6-31+G(d,p) and DFT/B97D/6-31+G(d,p) level were performed on neutral, positively charged, and negatively charged pentacene, while single-point energy calculations at the DFT/B97D/6-31+G(d,p) level were completed for neutral and negatively charged C_{60} using the Gaussian 09 software suite.[38] Additional information on force-field parametrization is available in ref 29.

As a first step to exploring the effects of an organic−organic interface on the polarization energy due to an excess charge carrier, we determined the polarization energies of the respective bulk materials. In our previous investigations of electronic polarization energy, the parametrization of the electrostatic component of the AMOEBA force field was carried out via *ab initio* MP2 calculations followed by a distributed multipole analysis (DMA) to generate atom-centered multipoles.[30,31] As shown in Figure S1, this parametrization procedure leads to the excess charge in the anion becoming localized to one portion of the C_{60} molecule. To obtain a charge distribution in which the charge is delocalized across the entirety of C_{60}, as one would expect from previous theoretical studies,[39,40] the parametrization of the electrostatic component was carried out using density functional theory at the B97D level.[41] This method results in the negative charge of the C_{60} radical anion being evenly distributed across the entire molecule; the charge distributions for the radical-anion and radical-cation states of pentacene, as in the MP2 calculations, are distributed symmetrically across the entire molecule. Additional details of the validation of this new parametrization procedure are available in the Supporting Information.

Considering a given cluster of molecules, the polarization energy is calculated using the Lyons model:[42]

$$P_+ = IE_{ss} - IE_g \quad (1)$$

where P_+ is the polarization energy due to a positive charge and IE is the solid-state or gas-phase ionization energy, respectively; there exists an analogous equation for the polarization due to a negative charge, P_-, involving the electron affinities. The bulk polarization energy is determined by increasing the radius of spherical clusters and plotting the calculated polarization energies versus $1/N^3$, where N is the number of molecules in the cluster, and extrapolating to an infinite system size.[30,42,43]

DOI: 10.1021/acsami.6b02851
ACS Appl. Mater. Interfaces 2016, 8, 15524−15534

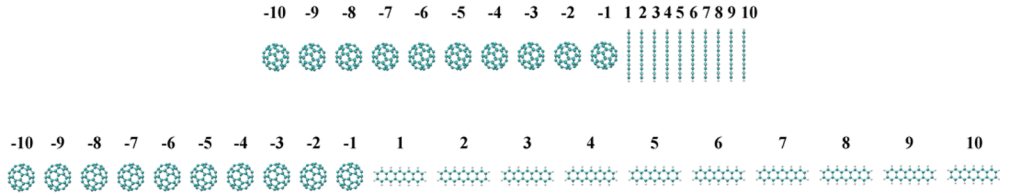

Figure 2. (Top) *Face-on* pentacene/C_{60} and (bottom) *edge-on* pentacene/C_{60} one-dimensional interfaces together with the numbering of the molecular sites. Note that only the six closest molecules to the interface have been considered for the polarization energy and induced-dipole calculations as additional molecules introduce artifacts from the organic−vacuum interface at the edges of the systems.

Model one-dimensional (1D) interfaces were constructed using the isolated geometries from above, wherein each pentacene or C_{60} was replicated along one dimension to give a stacked interface in either a *face-on* or *edge-on* configuration (Figure 2). While both of these configurations differ significantly from what is observed for the actual materials (i.e., within layers pentacene packs in a herringbone fashion and molecules do not sit perfectly on top of one another), these simplified interfaces allow for the limit of perfect order to be probed without introducing the complexity of molecular rotation. Molecules within the 1D interfaces are separated by 3.5 Å with a 3.5 Å separation at the pentacene/C_{60} interface. Additionally, possible band bending at the interface is evaluated by placing either a positive or negative charge at the interface and moving it toward the bulk.

Model pentacene(001)/C_{60}(001) three-dimensional (3D) interfaces were created by placing a C_{60}(001) slab (6.8 nm × 6.8 nm × 14 layers) on top of a pentacene (001) slab (6.8 nm × 6.8 nm × 8.6 nm) together with a large vacuum space along the z direction to limit supercell periodicity to the xy-plane, resulting in a cell of (x =) 6.8 nm × (y =) 6.8 nm × (z =) 50 nm. This was followed by a molecular mechanics MM3[44] minimization to optimize the separation distance at the interface. Following the methodology of Fu et al.,[21] we used this configuration as the initial configuration for molecular dynamics (MD) simulations in the NVT ensemble at 300 K with the velocity Verlet integrator[45] and Berendsen thermostat.[46] A spherical cutoff of 12 Å was implemented for the summation of van der Waals interactions and Ewald summation[47] for Coulomb interactions. The rattle algorithm[48] was employed to constrain C−H bonds. This system was equilibrated for 1 ns and then replicated in each of the x and y directions to give a final supercell of 13.7 nm × 13.7 nm × 50 nm composed of 4752 pentacene and 2744 C_{60} molecules. The supercell was then allowed to further evolve over 10 ps for final equilibration and over another 10 ps for data collection. The largest energy fluctuation during data collection was about 0.02% of the total energy with a standard deviation of less than 0.01%. Polarization energies at various sites at the interface and sites in layers moving away from the bulk were then calculated. All MD simulations were carried out using the Tinker code.[49]

RESULTS AND DISCUSSION

Bulk Polarization Energy. Since pentacene acts as an electron donor and C_{60} acts as an electron acceptor in the systems we wish to investigate, we first determine the bulk polarization energy due to a positive charge in pentacene and a negative charge in C_{60} via our revised parametrization procedure. While there have been a number of studies to determine the polarization energy due to a positive charge in pentacene,[35,50−53] evaluations of the polarization energy in C_{60} due to a positive or negative charge have been limited to the investigations of Sato and co-workers[54] and of Yoshida,[55] who evaluated the polarization energy in a series of fullerenes. Using the gas-phase and solid-state ionization energies determined by Lichtenberger and co-workers,[56] $P_{+,C_{60}}$ is 1.1−1.4 eV; by comparison to available gas-phase electron affinity (EA) data, $P_{-,C_{60}}$ is in the range of 1.4−1.6 eV; that is, it is either equal to or greater by up to 0.5 eV than $P_{+,C_{60}}$. These numbers suggest that $P_- \geq P_+$ in C_{60}, which is opposite of the trend observed for the unsubstituted linear oligoacenes, i.e., $P_- < P_+$.[30] This results from the absence of a molecular quadrupole in C_{60} and, thus, no contribution from charge-permanent quadrupole interactions. As a consequence, the polarization energy is determined mainly by induced-dipole interactions, though it is important to point out that higher-order charge-permanent multipole interactions occur. If one assumes an equal but oppositely signed charge distribution for the C_{60} anion and cation, then it is expected that $P_- = P_+$, which is one of the limits found experimentally (we note that, if the charge distributions are not equivalent and such that the cation is delocalizing more than the anion, a situation where $P_- > P_+$ would result due to larger induced dipoles near the regions with larger charge density). Indeed, we find that the charge distributions for the hole and electron are similar and opposite in sign. This results in a calculated polarization energy due to a negative charge carrier in C_{60} to be nearly equivalent to the polarization due to a positive charge carrier, 0.72 and 0.75 eV, respectively.

Experimentally, if we take for the polarization energy due to a negative charge carrier on a C_{60} molecule ($P_{-,C_{60}}$) the value of 1.4 eV at which $P_{+,C_{60}} = P_{-,C_{60}}$,[51,54] there is an estimated difference of about 0.2 eV with the polarization energy due to a positive charge carrier in pentacene ($P_{+,P5}$), 1.6 eV. Using our model, we calculated each of the respective bulk polarization energies through extrapolation of the polarization energy of finite clusters. We find that the polarization energy of a positive charge carrier in pentacene (0.99 eV) is calculated to be some 0.27 eV larger than that of a negative charge carrier in C_{60} (0.72 eV); see Figure 3. This is in general agreement with the calculations of D'Avino and co-workers, who applied both microelectrostatic and semiempirical models to the bulk of pentacene and C_{60} and obtained differences, $P_{+,P5} - P_{-,C_{60}}$, of 0.07 and 0.16 eV, respectively,[14] and the work of Gorczak et al.[13] who determined a difference of 0.31 eV.

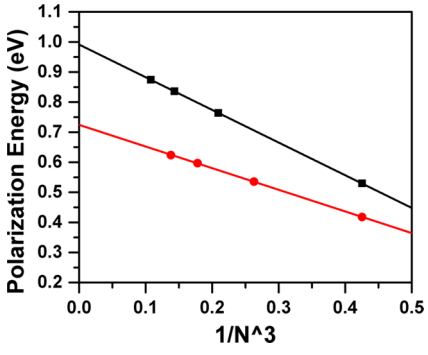

Figure 3. Electronic polarization energies for a positive charge in pentacene (black) and negative charge in C_{60} (red).

DOI: 10.1021/acsami.6b02851
ACS Appl. Mater. Interfaces 2016, 8, 15524−15534

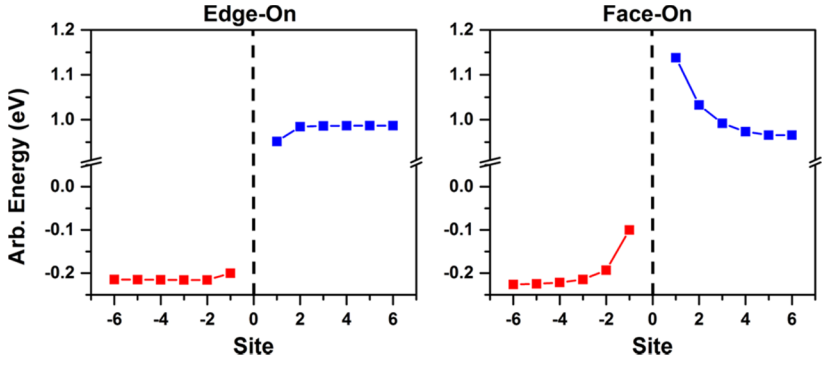

Figure 4. Shift in the ionization energy of pentacene (blue) and electron affinity of C_{60} (red) for an *edge-on* pentacene/C_{60} interface (left) and *face-on* pentacene/C_{60} interface (right). A more negative value for the EA represents a larger, i.e., more stabilizing, EA. For the IE, a more positive value represents a larger IE, i.e., less stabilizing.

Band Bending in One-Dimensional Stacks. To compare with previous theoretical results and provide an additional step of validation for our model,[9,10] we evaluated the band bending in the one-dimensional donor−acceptor chains illustrated in Figure 2. These 1D chains also allow us to use a step-up approach and examine how the interactions change as the complexity of the system increases. Within 1D model interfaces, we chose to have each molecule separated by 3.5 Å, so as to be consistent with the work of Idé et al.[57] We begin with a neutral system and then place a charge on either pentacene (site 1) or C_{60} (site −1) at the interface and move the charge to the nearest-neighbor away from the interface. At each site, the IE or EA is calculated as a function of molecular position (Figure 4). The same plot as a function of distance rather than site is available in Figure S2.

There is a destabilization of the electron on C_{60} as it is moved toward the interface for both orientations of pentacene, with the *face-on* pentacene configuration presenting a larger destabilization. This is a result of the larger interactions between a charge on C_{60} and the quadrupole on pentacene in the *face-on* orientation and the increased magnitude of the induced dipoles, as previously reported by Linares et al.[9] Also note, as we have recently shown,[29] that for the model chain of *edge-on* pentacenes, which is similar to the *inter*layer packing in bulk pentacene (packing along the *c*-axis), the band bending and thus the polarization energy changes very little after moving one layer from the interface (i.e., sites other than 1 or 2). For the *face-on* orientation, which is somewhat similar to the *intra*layer packing (*ab*-plane), the band bending falls off much more slowly, not saturating until the charge is on site-5 for pentacene; this is consistent with the behavior observed in the bulk, where the polarization energy does not stabilize until about 4 nm (~10 molecular sites in pentacene) from the charge carrier.[30] For pentacene, there is also a qualitative change in the band bending since a hole is destabilized at the interface for a *face-on* pentacene interface and stabilized at the *edge-on* interface. Again, this results from the change in charge−quadrupole interactions; in the *edge-on* orientation, the positively charged pentacene interacts with small positive quadrupoles on the neighboring pentacene while in the *face-on* orientation the charged pentacene interacts with a large negative quadrupole.[57] Thus, as the charge moves away from the interface in the *edge-on* system, there are additional destabilizing like-signed charge−quadrupole interactions, while in the *face-on* interfaces there are additional stabilizing opposite-signed charge−quadrupole interactions.

Looking more closely at the neutral systems, there is an induced dipole at the interface due to the quadrupole moment of pentacene, as discussed by Idé et al.[57] This induced dipole not only impacts the molecules at the interface but also induces dipole moments along the chain although with lessening strength as one moves away from the interface. Depending on the orientation of the pentacenes, the direction of the induced dipole is different as the sign of the quadrupole component closest to C_{60} changes, i.e., the induced dipole points toward the C_{60} bulk for *face-on* pentacene and toward the pentacene bulk for *edge-on* pentacene (Figure 5). Also note that the induced dipole is an order-of-magnitude smaller for the *edge-on* pentacene configuration, a result of the small quadrupole moment and larger distance between additional atom-centers.

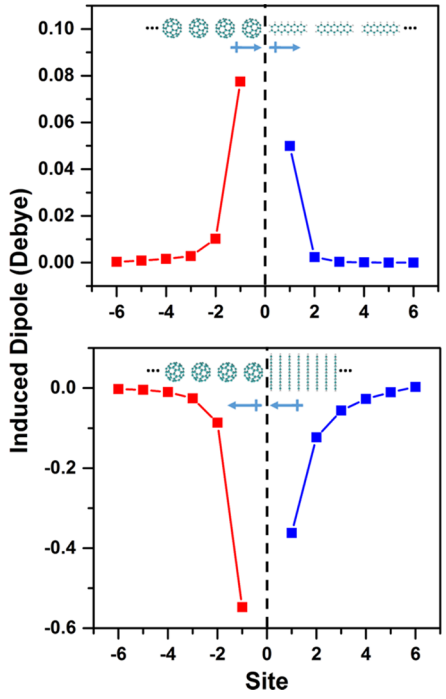

Figure 5. Induced dipoles on pentacene (blue) and C_{60} (red) at a model one-dimensional interface in the absence of any net charge, where each molecular site is separated by 3.5 Å in an *edge-on* orientation (top) and a *face-on* orientation (bottom). Inset: Illustration of the orientation of the induced dipoles of the interfacial molecules and representation of the molecular systems.

DOI: 10.1021/acsami.6b02851
ACS Appl. Mater. Interfaces 2016, 8, 15524−15534

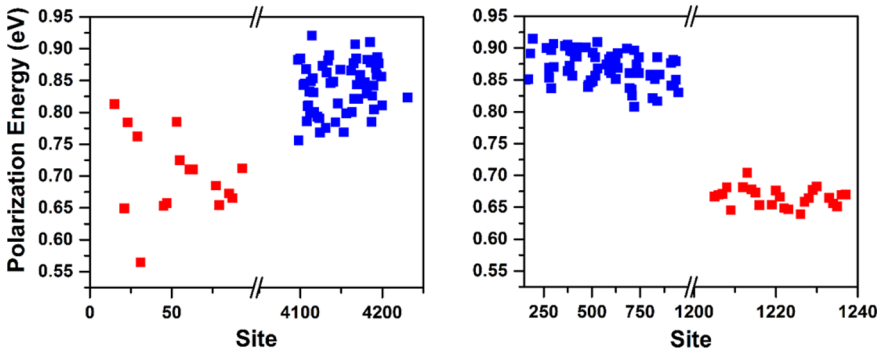

Figure 6. Polarization energy for a negative charge carrier in C_{60} (red) and a positive charge carrier in pentacene (blue) in the interfacial layers of the two organic components within spherical clusters with a 4 nm radius. Two systems are considered: (left) a slab of pentacene and a slab of C_{60} glued together followed by a MM3 minimization; (right) the same system after 1 ns of molecular dynamics simulation at 300 K.

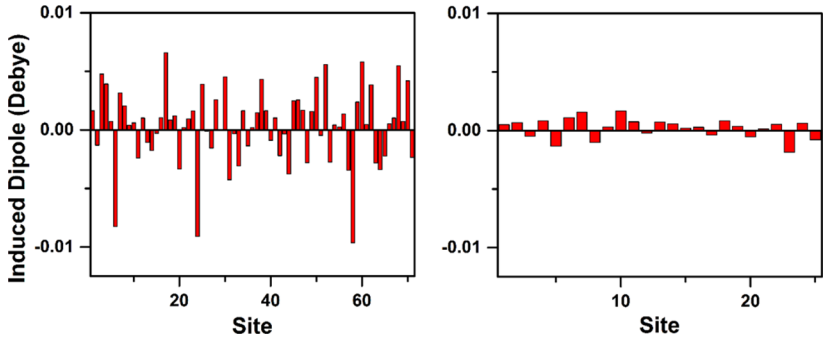

Figure 7. *z*-component of the induced dipole on pentacene (left) and C_{60} (right), as a function of molecular site at a neutral *edge-on* interface. Site numbers are arbitrary.

Thus, in the case of the model, highly ordered one-dimensional chains, it is found that the driving force for charges to move away from the interface is small for the *edge-on* pentacene orientation and quite large for the *face-on* orientation. These differences stem from a combination of permanent multipole and induced-dipole contributions. If the orientation of just a few molecules presents such pronounced effects on a charge at the interface, then the effects of many additional neighbors, resulting in variations in the electrostatic environment of each molecule, should be expected to have an important impact.

Polarization Energy and Induced Dipoles in Model Bilayer Interfaces. We now consider the polarization energies due to the presence of either a single positive or negative at an idealized *edge-on* pentacene/C_{60} interface, created by layering crystalline surfaces of pentacene and C_{60}, followed by minimization using the MM3 force field to optimize the *inter*molecular separation distances at the interface; see Figure S3. Even when examining such a static model interface,[9,12,13] it is readily seen in Figure 6 that there is a broad range of polarization energies within the interfacial layers of pentacene and C_{60}, making each site distinctive. For pentacene, the polarization energy due to a positive charge carrier in a 4 nm radius cluster ranges from 0.76 to 0.92 eV, while a negative charge carrier in C_{60} has a polarization stabilization between 0.56 and 0.81 eV.[58] The 0.2 to 0.3 eV range in polarization energy between sites suggests that the electrostatic environment of each molecule varies significantly due to the presence and packing configurations of the additional organic material.

The MD simulations of Fu et al. showed that the pentacene(001)/C_{60} interface (i.e., a *face-on* type interface) is more complex than is typically accounted for, with the pentacene molecules migrating from the interfacial layer to the divots between the neighboring C_{60} molecules, resulting in a mixed, disordered interface.[21] To provide a more complete picture than the static interface composed of two slabs brought to close contact, the MM3 force field was used for MD simulations to model a disordered interface due to the dynamic processes that occur at room temperature. The C_{60} molecules are found to take on a hexagonal closed packing configuration as reported previously.[21]

We considered 25 C_{60} and 71 pentacene molecules at the interface, extracted from a single MD snapshot after equilibration was reached, for comparison to the molecular-mechanics minimized static interface and analysis of how the interface changes after 1 ns of simulation at 300 K. Note that the molecular sites are not identical, as highlighted by the large variation in the induced dipole for sites along the interface (Figure 7). Note, also, that there does not appear to be a correlation between the sign and magnitude of the induced dipole of a specific site and other sites that are similar via visual inspection. The largest qualitative difference between the minimized slab interface and the interface after being treated by MD is the narrowing of the distribution of site polarization energies at the interface and an increase in the average difference between the polarization energies due to a positive or negative charge (0.14 eV, minimized; 0.21 eV, dynamic); the average polarization energy due to each charge type also increases by 0.1 eV. This indicates that during the MD simulations the thermal fluctuations act to minimize the overall differences among molecular sites, while still keeping them distinct. It is interesting to note that, while the site polarization energies are more uniform in the MD snapshot, the sites display a large number of configurations, including pentacene

DOI: 10.1021/acsami.6b02851
ACS Appl. Mater. Interfaces 2016, 8, 15524−15534

partially moving from the pentacene layer to the space between C_{60} molecules. These types of dislocations do not result in large changes in polarization energy but do impact charge separation as discussed later.

Using this same snapshot, we probe molecular sites as the charge is moved away from the interface toward the bulk to see how the polarization energy changes as a function of molecular layer; see Figure 8. First focusing on pentacene, we observe that

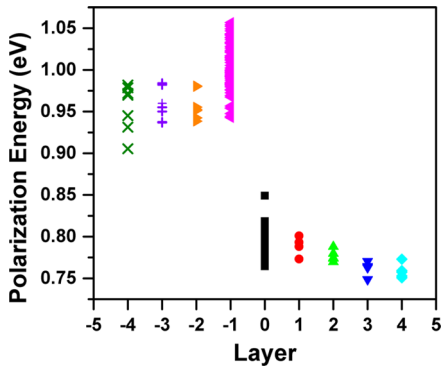

Figure 8. Polarization energy due to a positive charge in pentacene and negative charge in C_{60} as a function of molecular layer with respect to the interface. The C_{60} layers considered are the C_{60} interfacial layer (■, black), 1 layer from the interface (●, red), 2 layers from the interface (▲, green), 3 layers from the interface (▼, blue), and 4 layers from the interface (◆, cyan), with the latter approximating the bulk. The pentacene layers considered are the interfacial pentacene layer (◀, magenta), 1 layer from the interface (▶, orange), 2 layers from the interface (+, purple), and 3 layers from the interface (×, green), with the latter approximating the bulk.

there is a large change in the polarization energy when moving from the interfacial layer of pentacene to one layer from the interface and then little change upon moving farther from the interface. In contrast to an organic−vacuum interface, where the polarization energy at the interface is lower than the bulk (0.07 eV in tetracene),[29] the average polarization energy (1.00 eV, pentacene; 0.80 eV, C_{60}) at the considered organic−organic interface is larger than in the bulk (0.95 eV, pentacene; 0.76 eV, C_{60}). At the organic−vacuum interface, there is a reduction in the amount of stabilizing polarizable material and destabilizing permanent quadrupoles resulting in a net smaller polarization energy,[29] while at the pentacene/C_{60} interface, a polarizable material (i.e., C_{60}) is still present, but the destabilizing permanent quadrupoles that would have otherwise been present due to pentacene have been removed. Thus, there is a net increase in the polarization energy of sites along the pentacene/C_{60} interface.

A similar trend is seen on the C_{60} side of the interface. However, the polarization does not stabilize until the charge moves three layers away from the interface because the hexagonal closed packed configuration results in layers that are less well separated than in pentacene. Since the positive quadrupole component of the pentacene is pointed toward the C_{60} slab, the negative charge is more stabilized at the interface than in the bulk, which increases the polarization energy due to a negative charge at the interface, as observed for the one-dimensional systems.

While examining a single snapshot gives a picture of the disorder present at the interface at a single instance in time, we also follow the individual sites in time to determine how the dynamic nature of the environment of individual sites impacts the site polarization energies (Figure 9). We note the dynamic

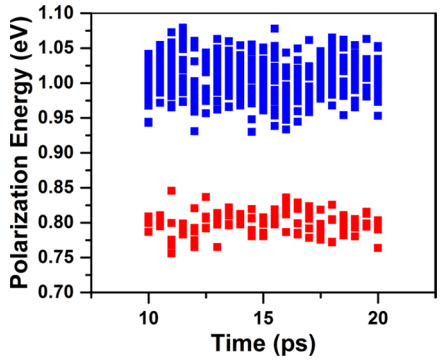

Figure 9. Polarization energies at selected sites of pentacene (blue) and C_{60} (red) as a function of time in 0.5 ps increments.

and static contributions to the disorder may also be determined, as Tummala et al. have recently done for a series of fullerenes,[59] although this is outside the scope of the current investigation. Snapshots were taken at 0.5 ps intervals where the polarization energy at five C_{60} sites and 19 pentacene sites was followed; each collection of sites on either side of the interface occupies a similar area. Compared to the single snapshot, the polarization energy distributions over the whole timespan are larger (the P_- distribution is 5% larger and the P_+ distribution is 30% larger), indicating that the environment of the pentacene sites vary much more than that of the C_{60} sites. While it is not unexpected that the polarization energy can vary by a large amount from site to site since the environment of each site is distinct, the large amount over which each individual site may change is an important feature. For C_{60}, the polarization energy of a given site is observed to vary by as much as 9% (0.07 eV) with respect to its smallest polarization energy, while the polarization energy of pentacene sites can vary by up to 12% (0.12 eV).

Interface Impact on Charge Separation. The process of exciton dissociation and charge separation is a highly debated topic in the literature.[60−67] The barrier, or lack thereof, to charge separation has been the focus of numerous articles with reports of barriers as large as 1.4 eV for charge separation in Alq_3 thin films to barriers of less than 10 meV in polymer/fullerene blends, where the charge carriers are expected to be largely delocalized.[64,68−73] Theoretical investigations report similar charge separation barriers and give insight into how intermolecular interactions affect this barrier:[12,13] (i) Yost and Van Voorhis[60] showed that, by modifying the bulk dielectric, molecular packing, and molecular multipole moments, the barrier to charge separation can be modified by shifting the direction and amount of band bending at the interface, which provides a driving force for charge separation; (ii) the interface geometry has been a significant focus of the work of Heremans and co-workers,[12] who report the barrier to charge separation at model pentacene/C_{60} interfaces to vary from 0.0 to 0.4 eV as a function of pentacene orientation; (iii) on the other hand, Grozema and co-workers[13] report a barrier to charge separation in an *edge-on* pentacene/C_{60} interface to be as large as 0.85 eV.

When a hole and electron are present at the interface, there are several interactions that occur: (i) Coulombic interactions between hole and electron; (ii) charge-permanent multipole interactions and charge-induced-dipole interactions between

DOI: 10.1021/acsami.6b02851
ACS Appl. Mater. Interfaces 2016, 8, 15524−15534

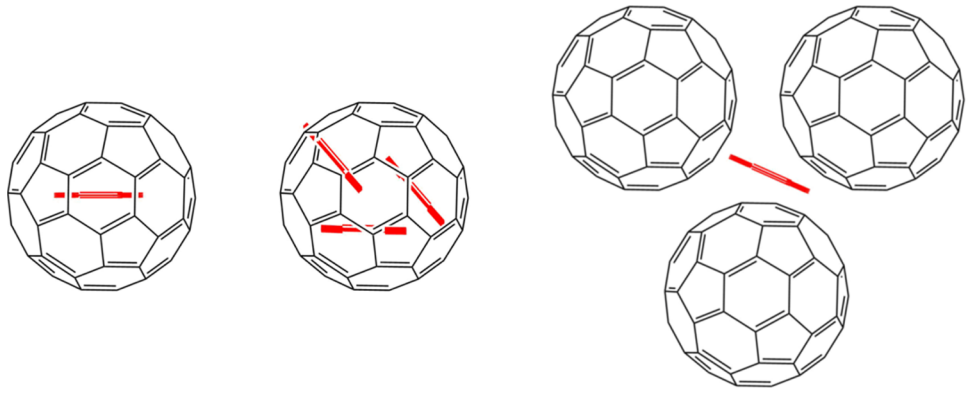

Figure 10. Top-down representations of the primary configurations of pentacene and C_{60} at the pentacene/C_{60} interface.

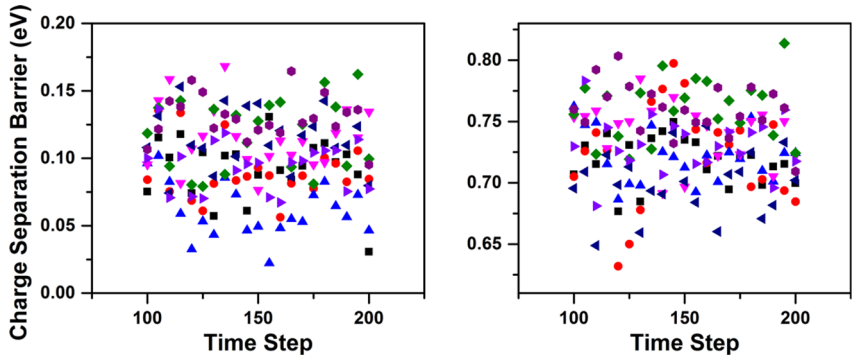

Figure 11. (Left) Charge separation barrier for a noninteracting electron−hole pair for eight pairs. (Right) Charge separation barrier for an interacting electron−hole pair for eight pairs. Symbols correspond to individual pentacene/C_{60} pairs as they are followed along the MD trajectory.

the charged molecules and their respective bulks; (iii) so-called mutual interactions due to the pentacene bulk seeing the negatively charged C_{60} and the C_{60} bulk seeing the positively charged pentacene, as well as the static and induced electrostatic interactions between the pentacene and C_{60} slabs that are not charged.

To provide insight into the charge separation process and the importance of accounting for the mutual interactions in addition to the Coulombic interactions, we have examined both an interacting electron−hole pair and a noninteracting electron−hole pair. The energy of a Coulombically bound electron−hole pair (E_{EH}) is defined as

$$E_{EH} = \Delta E_{pair} - IE_{gas} - EA_{gas} \quad (2)$$

where ΔE_{pair} is the change in energy of the system between the presence of the charge pair and the absence of the charge pair. The energy of a noninteracting electron−hole pair (E_{NI-EH}), that is when the electron and hole do not see each other, is simply the sum of the polarization energies:

$$E_{NI-EH} = P_+ + P_- \quad (3)$$

where P_+ and P_- may either correspond to the bulk or the interface. The comparison of E_{EH} and E_{NI-EH} allows the determination of the amount of mutual interaction. As we have done with the polarization energy of different molecular sites, we tracked each of these quantities along a MD trajectory to determine how the electrostatic environment of the electron−hole pair changes at a disordered interface as a function of time.

Note that there are three primary configurations of pentacene and C_{60} at the pentacene/C_{60} interface: a first one (Figure 10, left) where C_{60} sits directly on top of a pentacene, a second one (Figure 10, middle) where C_{60} sits above three neighboring pentacenes, and a third configuration (Figure 10, right) where a pentacene sits in the space below three C_{60} molecules.

Looking first, for simplicity, at a single snapshot from the MD trajectory and comparing the sites within this single frame, we observe that the charge separation barrier for an electron−hole pair ($E_{CS,EH}$), defined as the difference in E_{EH} evaluated at the interface and in the bulk, ranges from 0.70 to 0.76 eV. These values fall between the previously reported barriers of Grozema and co-workers (0.85 eV)[13] and Heremans and co-workers (0.44 eV).[12] Although the reported values cover a wide range of energies, it is important to note the differences in these models; while our results agree well with those of Grozema and co-workers, the microelectrostatic model underestimates the charge-separation barrier. This is likely due to two factors: (i) the submolecular representation of pentacene (described via five points) and C_{60} (described by 12 points in the microelectrostatic model), where these approximations in fact lead to an overestimation of the polarizability of the molecules and cause the respective bulk regions to overstabilize the excess charges, allowing for more facile charge separation,[9] and (ii) the treatment of Heremans and co-workers, which makes use of finite-sized spheres that are estimated to introduce approximately 10% error into the charge-induced dipole interactions.

By also evaluating the barrier for charge separation in a noninteracting electron−hole pair ($E_{CS,NI-EH}$), that is the difference between E_{NI-EH} evaluated at the interface and in the bulk, we can determine the magnitude of the Coulomb and mutual interactions that are key to properly describing the evolution from a Coulombically bound electron−hole pair to

DOI: 10.1021/acsami.6b02851
ACS Appl. Mater. Interfaces 2016, 8, 15524−15534

free charge carriers in the bulk. Looking at the same set of donor−acceptor sites as the interacting electron−hole pairs, we determine $E_{CS,NI-EH}$ to vary by as much as 0.13 eV from site-to-site and become as small as 0.02 eV. The fact that $E_{CS,NI-EH}$ never becomes negative, although it does come within thermal energy at room temperature (0.025 eV), highlights that, in the case of the pentacene(001)/C_{60} interface, the hole and electron are more stabilized at the interface than in the bulk.

By comparing $E_{CS,EH}$ and $E_{CS,NI-EH}$, the mutual interaction contribution, resulting from the hole, electron, and respective bulks interacting, to charge separation may be quantified. These mutual interactions account for the majority of the barrier to charge separation for the interacting pair, upward of 90% of $E_{CS,EH}$. Thus, it is the change in inductive and electrostatic interactions of the environment when the two opposite charges are near each other that dictates the charge separation barrier. To minimize the barrier to charge separation, it is then necessary to reduce the contributions from these mutual interactions. One approach is the use of a *face-on* pentacene orientation; however, as stated earlier, such an orientation has been theoretically calculated to cause a large increase in the rate of charge recombination.[11]

This single, static picture, though, does not fully comprehend the complexity of the pentacene/C_{60} interface, as the individual molecules move in time. For any given site, we observe that $E_{CS,EH}$ varies by as much as 0.17 eV, nearly as much as the largest differences in $E_{CS,EH}$ observed for all sites over a range of 10 ps (0.18 eV; from 0.63 to 0.81 eV, Figure 11). This large variation in the barrier to charge separation, while not large enough to suggest barrier-less charge separation at the pentacene/C_{60} interface, must be considered in addition to static pictures of the charge-separation energy. Furthermore, we can separate the pentacene/C_{60} pairs into two groups: (i) pentacenes that remain in the edge-on orientation with the neighboring fullerenes (Figure 10, left and center); (ii) pentacenes that intercalate (at least partially) into the fullerene layer (Figure 10, right). The edge-on pentacenes have limited movement (vibration within the layer), as they are constrained to the pentacene layer. Thus, the change in charge separation for these sites is relatively small, about 0.09 eV.

On the other hand, those pentacenes that are able to move partially into the fullerene layer experience a significant change in charge separation barrier. Over a period of about 7 ps, the pentacene can slide away from the pentacene interface, where the charge separation barrier is at a minimum due to the large distance between the hole and electron, to a position where approximately one fused ring is out of the pentacene layer, protruding into the C_{60} layer. At this latter position, the charge-separation barrier becomes large due to the closer proximity of the hole and electron. The pentacene can then translate back down to the pentacene layer. Along this course of motion, the charge-separation barrier can change by almost 0.2 eV (Figure S4).

This motion provides a more complex picture of charge separation in these systems by opening additional pathways for consideration. From a positively minded perspective, one could envision a scenario where a charge transfer state is formed when the pentacene is in a partially intercalated state, leading to a maximized electronic coupling; then, as the pentacene moves back into the pentacene domain, the hole can partially delocalize within this layer and the barrier to charge separation is reduced allowing for more easy separation of the hole and electron into free charge carriers.

SYNOPSIS

Through a combination of quantum-mechanics calculations and molecular-mechanics and molecular-dynamics simulations, we have investigated the effect of the bulk organic material and of an organic−organic interface on the energy of an excess charge carrier. By using molecular dynamics simulations, we have shown that a simple static picture of the interface between two organic slabs is not sufficient to properly describe the dynamic nature of these complex interfaces present in the active layers of OPV devices. In the bulk materials, we calculate that a positive charge in pentacene is more stabilized by its environment than a negative charge in C_{60} (by about 0.27 eV), in agreement with available experimental estimates; for both pentacene and C_{60}, an excess charge is more stabilized, i.e., has a larger polarization energy, at the interface than in the bulk, in contrast to the behavior observed at an organic−vacuum interface.[29]

Moving beyond simply gluing two organic slabs together, we examined a bulk *edge-on* pentacene/C_{60} interface after 1 ns of molecular dynamics simulation at room temperature to determine how the energetic landscape changes in time. From the results of these MD simulations, we obtain that

- Each site along the interface feels a unique electrostatic environment that determines its polarization energy and results from the instantaneous positions of all neighboring molecules.
- There exists a distribution of polarization energies at the interface, in contrast to the bulk where each site is essentially equivalent.
- In general, an excess charge at the pentacene/C_{60} interface is more stabilized than in the bulk; however, since the electrostatic environment of each site can change significantly in time, this does not always hold true.
- The barrier to charge separation for an electron−hole pair at the pentacene(001)/C_{60} interface is about 0.75 eV but can vary by as much as 25% for a given site in time.

Thus, a major conclusion that can be drawn is that the *dynamic* nature of the interface results in large changes in the energetic landscape on a short time scale, which must be accounted for in discussions of charge separation in OPV devices.

Our work underlines that the energetic landscape at a bilayer interface is more complex than is often considered, with the environment of each molecular site changing considerably over time. While the charge separation energies that we have reported here would seem to indicate that efficient charge separation is not possible in such bilayer configurations, we note that there are several effects that would act to reduce or negate this large barrier:

(i) As has been recently shown,[74] the static multipole moments at the interface can be tuned to promote efficient charge separation and lead to high-performance OPV devices.

(ii) By increasing the dimensionality of the charge transport in the active materials of OPVs, the entropy of the system can increase and result in more efficient charge separation.[75]

(iii) Charge delocalization would increase the mean distance between charge centers;[76,77] thus, delocalization combined with the changing barrier to charge separation, due to motions in and out of the molecular plane, can act to decrease the magnitude of the charge-separation barrier.

DOI: 10.1021/acsami.6b02851
ACS Appl. Mater. Interfaces 2016, 8, 15524−15534

Indeed, there are a number of interactions and phenomena that must be considered and accounted for in an integrated model if we are to understand in detail the processes that occur at organic−organic interfaces.

■ ASSOCIATED CONTENT

Supporting Information

The Supporting Information is available free of charge on the ACS Publications website at DOI: 10.1021/acsami.6b02851.

A qualitative description of the difference in overall system order in the minimized and MD interfaces, the single-molecule structures used for the parametrization of the AMOEBA force field, and the crystal structure of C_{60} generated via the Materials Studio suite. (PDF)

■ AUTHOR INFORMATION

Corresponding Authors

*E-mail: chad.risko@uky.edu.

*E-mail: jean-luc.bredas@kaust.edu.sa.

Notes

The authors declare no competing financial interest.

■ ACKNOWLEDGMENTS

This work has been supported by King Abdullah University of Science and Technology (KAUST), the KAUST Competitive Research Grant program, and the Office of Naval Research Global (Award N62909-15-1-2003). We acknowledge the IT Research Computing Team and Supercomputing Laboratory at KAUST for providing computational and storage resources. This work has also used the computing resources of the Garnet, Spirit, and Copper supercomputing systems through the DoD HPCMP. C.R. thanks the University of Kentucky Vice President of Research for start-up funds. We wish to thank Mahesh Kumar Ravva and Naga Rajesh Tummala for stimulating discussions and assistance with technical elements of the molecular dynamics simulations.

■ REFERENCES

(1) *NREL Best Research-Cell Efficiencies*; http://www.nrel.gov/ncpv/images/efficiency_chart.jpg (accessed April 13, 2016).

(2) *Heliatek Sets New Organic Photovoltaic World Record Efficiency of 13.2%*;http://www.heliatek.com/en/press/press-releases/details/heliatek-sets-new-organic-photovoltaic-world-record-efficiency-of-13-2 (accessed March 7, 2016).

(3) Zhao, J.; Li, Y.; Yang, G.; Jiang, K.; Lin, H.; Ade, H.; Ma, W.; Yan, H. Efficient Organic Solar Cells Processed from Hydrocarbon Solvents. *Nat. Energy* **2016**, *1*, 15027.

(4) Liu, Y.; Zhao, J.; Li, Z.; Mu, C.; Ma, W.; Hu, H.; Jiang, K.; Lin, H.; Ade, H.; Yan, H. Aggregation and Morphology Control Enables Multiple Cases of High-Efficiency Polymer Solar Cells. *Nat. Commun.* **2014**, *5*, 5293.

(5) Hu, H.; Jiang, K.; Yang, G.; Liu, J.; Li, Z.; Lin, H.; Liu, Y.; Zhao, J.; Zhang, J.; Huang, F.; Qu, Y.; Ma, W.; Yan, H. Terthiophene-Based D−A Polymer with an Asymmetric Arrangement of Alkyl Chains That Enables Efficient Polymer Solar Cells. *J. Am. Chem. Soc.* **2015**, *137*, 14149−14157.

(6) Bredas, J. L.; Norton, J. E.; Cornil, J.; Coropceanu, V. Molecular Understanding of Organic Solar Cells: The Challenges. *Acc. Chem. Res.* **2009**, *42*, 1691−1699.

(7) Lyons, B. P.; Clarke, N.; Groves, C. The Relative Importance of Domain Size, Domain Purity and Domain Interfaces to the Performance of Bulk-Heterojunction Organic Photovoltaics. *Energy Environ. Sci.* **2012**, *5*, 7657−7663.

(8) Yan, H.; Swaraj, S.; Wang, C.; Hwang, I.; Greenham, N. C.; Groves, C.; Ade, H.; McNeill, C. R. Influence of Annealing and Interfacial Roughness on the Performance of Bilayer Donor/Acceptor Polymer Photovoltaic Devices. *Adv. Funct. Mater.* **2010**, *20*, 4329−4337.

(9) Linares, M.; Beljonne, D.; Cornil, J. r. m.; Lancaster, K.; Brédas, J.-L.; Verlaak, S.; Mityashin, A.; Heremans, P.; Fuchs, A.; Lennartz, C.; Idé, J.; Méreau, R. l.; Aurel, P.; Ducasse, L.; Castet, F. d. r. On the Interface Dipole at the Pentacene−Fullerene Heterojunction: A Theoretical Study. *J. Phys. Chem. C* **2010**, *114*, 3215−3224.

(10) Mothy, S.; Guillaume, M.; Idé, J.; Castet, F.; Ducasse, L.; Cornil, J.; Beljonne, D. Tuning the Interfacial Electronic Structure at Organic Heterojunctions by Chemical Design. *J. Phys. Chem. Lett.* **2012**, *3*, 2374−2378.

(11) Yi, Y. P.; Coropceanu, V.; Bredas, J. L. Exciton-Dissociation and Charge-Recombination Processes in Pentacene/C60Solar Cells. *J. Am. Chem. Soc.* **2009**, *131*, 15777−15783.

(12) Verlaak, S.; Beljonne, D.; Cheyns, D.; Rolin, C.; Linares, M.; Castet, F.; Cornil, J.; Heremans, P. Electronic Structure and Geminate Pair Energetics at Organic−Organic Interfaces: The Case of Pentacene/C60 Heterojunctions. *Adv. Funct. Mater.* **2009**, *19*, 3809−3814.

(13) Gorczak, N.; Swart, M.; Grozema, F. C. Energetics of Charges in Organic Semiconductors and at Organic Donor-Acceptor Interfaces. *J. Mater. Chem. C* **2014**, *2*, 3467−3475.

(14) Castet, F.; D'Avino, G.; Muccioli, L.; Cornil, J.; Beljonne, D. Charge Separation Energetics at Organic Heterojunctions: On the Role of Structural and Electrostatic Disorder. *Phys. Chem. Chem. Phys.* **2014**, *16*, 20279−20290.

(15) Beljonne, D.; Cornil, J.; Muccioli, L.; Zannoni, C.; Bredas, J. L.; Castet, F. Electronic Processes at Organic-Organic Interfaces: Insight from Modeling and Implications for Opto-electronic Devices. *Chem. Mater.* **2011**, *23*, 591−609.

(16) Chen, W.; Nikiforov, M. P.; Darling, S. B. Morphology Characterization in Organic and Hybrid Solar Cells. *Energy Environ. Sci.* **2012**, *5*, 8045−8074.

(17) Liao, H.-C.; Ho, C.-C.; Chang, C.-Y.; Jao, M.-H.; Darling, S. B.; Su, W.-F. Additives for Morphology Control in High-Efficiency Organic Solar Cells. *Mater. Today* **2013**, *16*, 326−336.

(18) Coakley, K. M.; McGehee, M. D. Conjugated Polymer Photovoltaic Cells. *Chem. Mater.* **2004**, *16*, 4533−4542.

(19) Casalegno, M.; Carbonera, C.; Luzzati, S.; Raos, G. Coarse-Grained Kinetic Modelling of Bilayer Heterojunction Organic Solar Cells. *Org. Electron.* **2012**, *13*, 750−761.

(20) Bartelt, J. A.; Beiley, Z. M.; Hoke, E. T.; Mateker, W. R.; Douglas, J. D.; Collins, B. A.; Tumbleston, J. R.; Graham, K. R.; Amassian, A.; Ade, H.; Fréchet, J. M. J.; Toney, M. F.; McGehee, M. D. The Importance of Fullerene Percolation in the Mixed Regions of Polymer−Fullerene Bulk Heterojunction Solar Cells. *Adv. Energy Mater.* **2013**, *3*, 364−374.

(21) Fu, Y.-T.; Risko, C.; Brédas, J.-L. Intermixing at the Pentacene-Fullerene Bilayer Interface: A Molecular Dynamics Study. *Adv. Mater.* **2013**, *25*, 878−882.

(22) Correia, H. M. G.; Barbosa, H. M. C.; Marques, L.; Ramos, M. M. D. Understand the Importance of Molecular Organization at Polymer−Polymer Interfaces in Excitonic Solar Cells. *Thin Solid Films* **2014**, *560*, 59−64.

(23) Bloking, J. T.; Giovenzana, T.; Higgs, A. T.; Ponec, A. J.; Hoke, E. T.; Vandewal, K.; Ko, S.; Bao, Z.; Sellinger, A.; McGehee, M. D. Comparing the Device Physics and Morphology of Polymer Solar Cells Employing Fullerenes and Non-Fullerene Acceptors. *Adv. Energy Mater.* **2014**, *4*, 1301426.

(24) Mladenović, M.; Vukmirović, N. Charge Carrier Localization and Transport in Organic Semiconductors: Insights from Atomistic Multiscale Simulations. *Adv. Funct. Mater.* **2015**, *25*, 1915−1932.

(25) Gehrig, D. W.; Howard, I. A.; Sweetnam, S.; Burke, T. M.; McGehee, M. D.; Laquai, F. The Impact of Donor−Acceptor Phase Separation on the Charge Carrier Dynamics in pBTTT:PCBM Photovoltaic Blends. *Macromol. Rapid Commun.* **2015**, *36*, 1054−1060.

(26) Buchaca-Domingo, E.; Vandewal, K.; Fei, Z.; Watkins, S. E.; Scholes, F. H.; Bannock, J. H.; de Mello, J. C.; Richter, L. J.; DeLongchamp, D. M.; Amassian, A.; Heeney, M.; Salleo, A.; Stingelin, N. Direct Correlation of Charge Transfer Absorption with Molecular Donor:Acceptor Interfacial Area via Photothermal Deflection Spectroscopy. *J. Am. Chem. Soc.* **2015**, *137*, 5256−5259.
(27) Noriega, R.; Rivnay, J.; Vandewal, K.; Koch, F. P. V.; Stingelin, N.; Smith, P.; Toney, M. F.; Salleo, A. A General Relationship Between Disorder, Aggregation and Charge Transport in Conjugated Polymers. *Nat. Mater.* **2013**, *12*, 1038−1044.
(28) Collins, B. A.; Tumbleston, J. R.; Ade, H. Miscibility, Crystallinity, and Phase Development in P3HT/PCBM Solar Cells: Toward an Enlightened Understanding of Device Morphology and Stability. *J. Phys. Chem. Lett.* **2011**, *2*, 3135−3145.
(29) Ryno, S. M.; Risko, C.; Bredas, J. L. Impact of Molecular Orientation and Packing Density on Electronic Polarization in the Bulk and at Surfaces of Organic Semiconductors. *ACS Appl. Mater. Interfaces* **2016**, DOI: 10.1021/acsami.6b02579.
(30) Ryno, S. M.; Lee, S. R.; Sears, J.; Risko, C.; Bredas, J. L. Electronic Polarization Effects upon Charge Injection in Oligoacene Molecular Crystals: Description via a Polarizable Force Field. *J. Phys. Chem. C* **2013**, *117*, 13853−13860.
(31) Ryno, S. M.; Risko, C.; Brédas, J.-L. Impact of Molecular Packing on Electronic Polarization in Organic Crystals: The Case of Pentacene vs TIPS-Pentacene. *J. Am. Chem. Soc.* **2014**, *136*, 6421−6427.
(32) Ren, P.; Ponder, J. W. Consistent Treatment of Inter- and Intramolecular Polarization in Molecular Mechanics Calculations. *J. Comput. Chem.* **2002**, *23*, 1497−1506.
(33) Ponder, J. W.; Wu, C.; Ren, P.; Pande, V. S.; Chodera, J. D.; Schnieders, M. J.; Haque, I.; Mobley, D. L.; Lambrecht, D. S.; DiStasio, R. A.; Head-Gordon, M.; Clark, G. N. I.; Johnson, M. E.; Head-Gordon, T. Current Status of the AMOEBA Polarizable Force Field. *J. Phys. Chem. B* **2010**, *114*, 2549−2564.
(34) Allen, F. H. The Cambridge Structural Database: A Quarter Million Crystal Structures and Rising. *Acta Crystallogr., Sect. B: Struct. Sci.* **2002**, *B58*, 380−388.
(35) Mattheus, C. C.; Dros, A. B.; Baas, J.; Meetsma, A.; Boer, J. L. d.; Palstra, T. T. M. Polymorphism in Pentacene. *Acta Crystallogr., Sect. C: Cryst. Struct. Commun.* **2001**, *57*, 939.
(36) Bürgi, H.-B.; Blanc, E.; Schwarzenbach, D.; Liu, S.; Lu, Y.-j.; Kappes, M. M.; Ibers, J. A. The Structure of C60: Orientational Disorder in the Low-Temperature Modification of C60. *Angew. Chem., Int. Ed. Engl.* **1992**, *31*, 640−643.
(37) Stone, A. J. Distributed Multipole Analysis: Stability for Large Basis Sets. *J. Chem. Theory Comput.* **2005**, *1*, 1128−1132.
(38) Frisch, M. J.; Trucks, G. W.; Schlegel, H. B.; Scuseria, G. E.; Robb, M. A.; Cheeseman, J. R.; Scalmani, G.; Barone, V.; Mennucci, B.; Petersson, G. A.; Nakatsuji, H.; Caricato, M.; Li, X.; Hratchian, H. P.; Izmaylov, A. F.; Bloino, J.; Zheng, G.; Sonnenberg, J. L.; Hada, M.; Ehara, M.; Toyota, K.; Fukuda, R.; Hasegawa, J.; Ishida, M.; Nakajima, T.; Honda, Y.; Kitao, O.; Nakai, H.; Vreven, T.; Montgomery, J. A., Jr.; Peralta, J. E.; Ogliaro, F.; Bearpark, M. J.; Heyd, J.; Brothers, E. N.; Kudin, K. N.; Staroverov, V. N.; Kobayashi, R.; Normand, J.; Raghavachari, K.; Rendell, A. P.; Burant, J. C.; Iyengar, S. S.; Tomasi, J.; Cossi, M.; Rega, N.; Millam, N. J.; Klene, M.; Knox, J. E.; Cross, J. B.; Bakken, V.; Adamo, C.; Jaramillo, J.; Gomperts, R.; Stratmann, R. E.; Yazyev, O.; Austin, A. J.; Cammi, R.; Pomelli, C.; Ochterski, J. W.; Martin, R. L.; Morokuma, K.; Zakrzewski, V. G.; Voth, G. A.; Salvador, P.; Dannenberg, J. J.; Dapprich, S.; Daniels, A. D.; Farkas, Ö.; Foresman, J. B.; Ortiz, J. V.; Cioslowski, J.; Fox, D. J. *Gaussian 09*; Gaussian, Inc.: Wallingford, CT, USA, 2009.
(39) Gastel, M. v. Zero-Field Splitting of the Lowest Excited Triplet States of C60 and C70 and Benzene. *J. Phys. Chem. A* **2010**, *114*, 10864−10870.
(40) Green, W. H.; Gorun, S. M.; Fitzgerald, G.; Fowler, P. W.; Ceulemans, A.; Titeca, B. C. Electronic Structures and Geometries of C60 Anions via Density Functional Calculations. *J. Phys. Chem.* **1996**, *100*, 14892−14898.
(41) Note that previous electronic-structure calculations have shown the calculated charge distribution of fullerene anion to be highly sensitive to the amount of included Hartree−Fock exchange.
(42) Lyons, L. Ionized States of Molecular Crystals. *Aust. J. Chem.* **1957**, *10*, 365−367.
(43) Silinsh, E. A. *Organic Molecular Crystals: Their Electronic States*; Springer: New York, 1980.
(44) Lii, J. H.; Allinger, N. L. Molecular Mechanics. The MM3 Force Field for Hydrocarbons. 3. The van der Waals' Potentials and Crystal Data for Aliphatic and Aromatic Hydrocarbons. *J. Am. Chem. Soc.* **1989**, *111*, 8576−8582.
(45) Swope, W. C.; Andersen, H. C.; Berens, P. H.; Wilson, K. R. A Computer Simulation Method for the Calculation of Equilibrium Constants for the Formation of Physical Clusters of Molecules: Application to Small Water Clusters. *J. Chem. Phys.* **1982**, *76*, 637−649.
(46) Berendsen, H. J. C.; Postma, J. P. M.; van Gunsteren, W. F.; DiNola, A.; Haak, J. R. Molecular Dynamics with Coupling to an External Bath. *J. Chem. Phys.* **1984**, *81*, 3684−3690.
(47) Darden, T.; York, D.; Pedersen, L. Particle Mesh Ewald: An N·log(N) Method for Ewald Sums in Large Systems. *J. Chem. Phys.* **1993**, *98*, 10089−10092.
(48) Andersen, H. C. Rattle: A "Velocity" Version of the Shake Algorithm for Molecular Dynamics Calculations. *J. Comput. Phys.* **1983**, *52*, 24−34.
(49) Ponder, J. W. *TINKER: Software Tools for Molecular Design*; 2015. http://dasher.wustl.edu/tinker/. Ponder, J. W.; Richards, R. M. An Efficient Newton-Like Method for Molecular Mechanics Energy Minimization of Large Molecules. *J. Comput. Chem.* **1987**, *8*, 1016−1024. Kundrot, K. E.; Ponder, J. W.; Richards, F. M. Algorithms for Calculating Excluded Volume and its Derivatives as a Function of Molecular Conformation and Their Use in Energy Minimization. *J. Comput. Chem.* **1991**, *12*, 402−409.
(50) Sato, N.; Seki, K.; Inokuchi, H. Polarization Energies of Organic Solids Determined by Ultraviolet Photoelectron Spectroscopy. *J. Chem. Soc., Faraday Trans. 2* **1981**, *77*, 1621−1633.
(51) Sato, N.; Inokuchi, H.; Silinsh, E. A. Reevaluation of Electronic Polarization Energies in Organic Molecular Crystals. *Chem. Phys.* **1987**, *115*, 269−277.
(52) Qi, Y.; Mohapatra, S. K.; Kim, S. B.; Barlow, S.; Marder, S. R.; Kahn, A. Solution Doping of Organic Semiconductors Using Air-Stable n-Dopants. *Appl. Phys. Lett.* **2012**, *100*, 083305.
(53) Chan, C.; Kahn, A. N-Doping of Pentacene by Decamethylcobaltocene. *Appl. Phys. A: Mater. Sci. Process.* **2009**, *95*, 7−13.
(54) Sato, N.; Saito, Y.; Shinohara, H. Threshold Ionization Energy of C60 in the Solid State. *Chem. Phys.* **1992**, *162*, 433−438.
(55) Yoshida, H. Low-Energy Inverse Photoemission Study on the Electron Affinities of Fullerene Derivatives for Organic Photovoltaic Cells. *J. Phys. Chem. C* **2014**, *118*, 24377−24382.
(56) Lichtenberger, D. L.; Nebesny, K. W.; Ray, C. D.; Huffman, D. R.; Lamb, L. D. Valence and Core Photoelectron Spectroscopy of C60, Buckminsterfullerene. *Chem. Phys. Lett.* **1991**, *176*, 203−208.
(57) Idé, J.; Mothy, S.; Savoyant, A.; Fritsch, A.; Aurel, P.; Méreau, R.; Ducasse, L.; Cornil, J.; Beljonne, D.; Castet, F. Interfacial Dipole and Band Bending in Model Pentacene/C60 Heterojunctions. *Int. J. Quantum Chem.* **2013**, *113*, 580−584.
(58) We note that there is an approximately 10% error associated with using the polarization energy of a finite-sized sphere instead of the extrapolated values, as is typically done for the bulk, in this analysis.
(59) Tummala, N. R.; Zheng, Z.; Aziz, S. G.; Coropceanu, V.; Brédas, J.-L. Static and Dynamic Energetic Disorders in the C60, PC61BM, C70, and PC71BM Fullerenes. *J. Phys. Chem. Lett.* **2015**, *6*, 3657−3662.
(60) Yost, S. R.; Van Voorhis, T. Electrostatic Effects at Organic Semiconductor Interfaces: A Mechanism for "Cold" Exciton Breakup. *J. Phys. Chem. C* **2013**, *117*, 5617−5625.

(61) Heeger, A. J. 25th Anniversary Article: Bulk Heterojunction Solar Cells: Understanding the Mechanism of Operation. *Adv. Mater.* **2014**, *26*, 10−28.
(62) Tvingstedt, K.; Vandewal, K.; Zhang, F.; Inganäs, O. On the Dissociation Efficiency of Charge Transfer Excitons and Frenkel Excitons in Organic Solar Cells: A Luminescence Quenching Study. *J. Phys. Chem. C* **2010**, *114*, 21824−21832.
(63) Jailaubekov, A. E.; Willard, A. P.; Tritsch, J. R.; Chan, W.-L.; Sai, N.; Gearba, R.; Kaake, L. G.; Williams, K. J.; Leung, K.; Rossky, P. J.; Zhu, X. Y. Hot Charge-Transfer Excitons Set the Time Limit for Charge Separation at Donor/Acceptor Interfaces in Organic Photovoltaics. *Nat. Mater.* **2013**, *12*, 66−73.
(64) Clarke, T. M.; Durrant, J. R. Charge Photogeneration in Organic Solar Cells. *Chem. Rev.* **2010**, *110*, 6736−6767.
(65) Deibel, C.; Strobel, T.; Dyakonov, V. Role of the Charge Transfer State in Organic Donor−Acceptor Solar Cells. *Adv. Mater.* **2010**, *22*, 4097−4111.
(66) Etzold, F.; Howard, I. A.; Mauer, R.; Meister, M.; Kim, T.-D.; Lee, K.-S.; Baek, N. S.; Laquai, F. Ultrafast Exciton Dissociation Followed by Nongeminate Charge Recombination in PCDTBT:PCBM Photovoltaic Blends. *J. Am. Chem. Soc.* **2011**, *133*, 9469−9479.
(67) Vandewal, K.; Albrecht, S.; Hoke, E. T.; Graham, K. R.; Widmer, J.; Douglas, J. D.; Schubert, M.; Mateker, W. R.; Bloking, J. T.; Burkhard, G. F.; Sellinger, A.; Fréchet, J. M. J.; Amassian, A.; Riede, M. K.; McGehee, M. D.; Neher, D.; Salleo, A. Efficient Charge Generation by Relaxed Charge-Transfer States at Organic Interfaces. *Nat. Mater.* **2014**, *13*, 63−68.
(68) Hill, I. G.; Kahn, A.; Soos, Z. G.; Pascal, R. A., Jr. Charge-Separation Energy in Films of π-Conjugated Organic Molecules. *Chem. Phys. Lett.* **2000**, *327*, 181−188.
(69) Pensack, R. D.; Asbury, J. B. Barrierless Free Carrier Formation in an Organic Photovoltaic Material Measured with Ultrafast Vibrational Spectroscopy. *J. Am. Chem. Soc.* **2009**, *131*, 15986−15987.
(70) Deibel, C.; Strobel, T.; Dyakonov, V. Origin of the Efficient Polaron-Pair Dissociation in Polymer-Fullerene Blends. *Phys. Rev. Lett.* **2009**, *103*, 036402.
(71) Durrant, J. R. Molecular Approaches to Solar Energy Conversion: The Energetic Cost of Charge Separation from Molecular-Excited States. *Philos. Trans. R. Soc., A* **2013**, *371*, 20120195.
(72) Murthy, D. H. K.; Gao, M.; Vermeulen, M. J. W.; Siebbeles, L. D. A.; Savenije, T. J. Mechanism of Mobile Charge Carrier Generation in Blends of Conjugated Polymers and Fullerenes: Significance of Charge Delocalization and Excess Free Energy. *J. Phys. Chem. C* **2012**, *116*, 9214−9220.
(73) Jeong, K. S.; Pensack, R. D.; Asbury, J. B. Vibrational Spectroscopy of Electronic Processes in Emerging Photovoltaic Materials. *Acc. Chem. Res.* **2013**, *46*, 1538−1547.
(74) Poelking, C.; Tietze, M.; Elschner, C.; Olthof, S.; Hertel, D.; Baumeier, B.; Würthner, F.; Meerholz, K.; Leo, K.; Andrienko, D. Impact of Mesoscale Order on Open-Circuit Voltage in Organic Solar Cells. *Nat. Mater.* **2015**, *14*, 434−439.
(75) Gregg, B. A. Entropy of Charge Separation in Organic Photovoltaic Cells: The Benefit of Higher Dimensionality. *J. Phys. Chem. Lett.* **2011**, *2*, 3013−3015.
(76) Yoshida, H.; Yamada, K.; Tsutsumi, J. y.; Sato, N. Complete Description of Ionization Energy and Electron Affinity in Organic Solids: Determining Contributions from Electronic Polarization, Energy Band Dispersion, and Molecular Orientation. *Phys. Rev. B: Condens. Matter Mater. Phys.* **2015**, *92*, 075145.
(77) Bakulin, A. A.; Rao, A.; Pavelyev, V. G.; van Loosdrecht, P. H. M.; Pshenichnikov, M. S.; Niedzialek, D.; Cornil, J.; Beljonne, D.; Friend, R. H. The Role of Driving Energy and Delocalized States for Charge Separation in Organic Semiconductors. *Science* **2012**, *335*, 1340−1344.

DOI: 10.1021/acsami.6b02851
ACS Appl. Mater. Interfaces 2016, 8, 15524−15534